Simultaneous determination of 4-aminophenol and paracetamol based on CS-Ni nanocomposite-modified screen-printed disposable electrodes

Sarra Abdi[1] · Mohamed Lyamine Chelaghmia[1] · Rafiaa Kihal[1,2] · Craig E. Banks[3] · Alejandro Garcia-Miranda Ferrari[3] · Hassina Fisli[4] · Mouna Nacef[1] · Abed Mohamed Affoune[1] · Mohamed E. H. Benhamza[1]

Abstract

In the present work, chitosan-coated nickel nanoparticles (CS-Ni) were successfully prepared onto screen-printed electrode (SPE) by electrodeposition method with the assistance of an anionic surfactant of sodium dodecyl sulfate (SDS) for the individual and simultaneous sensing of 4-aminophenol (4-AP) and paracetamol (PA). The as-prepared sensor was characterized via scanning electron microscopy, X-ray diffraction, and fourier transform infrared techniques. The electrochemical catalytic behaviors of the 4-AP and PA on the fabricated NiNPs-SDS/CS/SPE electrode were explored using cyclic voltammetry (CV), differential pulse voltammetry (DPV), and electrochemical impedance spectroscopy (EIS). The NiNPS-SDS/CS modified screen-printed electrode demonstrated excellent electrocatalytic activity for 4-AP and PA, indicating that nickel microstructures have a high specific surface area, excellent electrical conductivity, and high electrocatalytic activity. The results indicate that CV and DPV could be easily applied to determine 4-AP and PA using the fabricated sensor under optimized conditions. However, CV is preferred for both analysts' sensing, with the largest linear range from 1 to 500 μM for 4-AP (R^2 = 0.999) and 1 μM to 2 mM (R^2 = 0.997) for PA, respectively. In terms of sensitivity and detection limit, DPVs response appeared to be a better technique choice, as it revealed the highest sensitivity values of 0.959 μA μM^{-1} cm^{-2} for 4-AP and 1.163 μA μM^{-1} cm^{-2} for PA, with the lowest detection limits of 0.06 and 0.04 μM for 4-AP and PA (S/N = 3), respectively. With a high recovery rate, good selectivity, excellent reproducibility, and strong anti-interference ability, the modified sensor was successfully applied to the simultaneous detection of 4-AP and PA in pharmaceutical tablets. It is expected to be widely used in actual sample detection.

Keywords Nickel nanoparticles · Sodium dodecyl sulfate · Electrochemical sensor · Cyclic voltammetry · Screen-printed electrode

Introduction

Due to its analgesic and antipyretic properties, paracetamol (4-acetaminophen or *N*-acetyl-*p*-aminophenol, PA) is one of the most commonly prescribed drugs worldwide. It treats fevers and pains, including muscular aches, headaches, toothaches, migraine, back pains, and chronic pains [1]. The maximum PA content in adult pharmaceutical products is typically around 4000 mg daily. On the other hand, an overdose of paracetamol can result in serious complications such as hepatotoxicity, nephrotoxicity, and pancreatic diseases [2].

The primary hydrolytic degradation product of paracetamol is 4-aminophenol (*p*-aminophenol, 4-AP) [3]. 4-AP causes harm to humans by raising body temperature over time. Several studies have also shown that it is nephrotoxic and teratogenic. According to the European, United States, and Chinese pharmacopeias, the recommended dose of 4-AP that can be safely administered in pharmaceuticals is 50 ppm (0.005%, w/w) [4]. Given the importance of 4-AP and PA in human life, simple, sensitive, and accurate analytical methods for simultaneous detection are required. High-performance liquid chromatography (HPLC), chemiluminescence, capillary electrophoresis, spectrophotometry, flow injection, titrimetry, colorimetry, gas chromatography, and mass spectroscopy have all been used to determine 4-AP and PA [1, 2].

However, these instrumentation methods have some limitations and drawbacks, such as a high cost, a lengthy and difficult detection procedure, and the requirement for well-equipped skilled personnel. These methods are also unreliable regarding reproducibility, selectivity, and sensitivity, making them unsuitable for routine detection of 4-AP and PA. To address these issues, electrochemical methods have recently piqued the interest of analytical and biomedical researchers due to their numerous advantages, such as low cost, ease of operation, excellent selectivity, and high stability compared to previously described methods [5, 6]. Because 4-AP and PA are electroactive molecules that can be oxidized electrochemically, electrochemical sensors may be a better option for quickly detecting and quantifying them.

Screen-printed electrodes (SPEs) have recently gained popularity in the field of electroanalysis for the fabrication of electrochemical sensors due to their numerous advantages such as simple fabrication, small size, low cost, portability, large-scale production, availability, speed, and sensitive real-time detection of an analyte without any pretreatment [7, 8]. Screen-printed electrodes typically have three electrodes: working, counter, and pseudo-reference. The working electrode is the most important of the three electrodes for conducting electrochemical reactions. It can be created using various inks (such as carbon, gold, and silver) on various substrates, including ceramic, plastic, and printed circuits [9, 10].

Counter and reference electrodes are typically made of graphite and silver inks. Screen printing offers a wider range of electrode designs, material compatibility, modification options, and mass-produced, cost-effective, and highly repeatable sensors compared to other solid carbon electrode substrates [11]. As a result, electrochemically modifying SPE with various nanomaterials, particularly inorganic nanoparticles, surfactants, and biopolymers, could be a useful technique for producing specific and selective electrochemical sensors for the simultaneous detection of 4-AP and PA [8]. Nickel (Ni) as a transition metal is one of the most important modifying agents among the various inorganic nanoparticles due to its good electrochemical stability, low cost, and high electrocatalytic activity towards the oxidation of some organic compounds when compared to other catalysts, particularly noble metals [12–17].

Surfactants are widely used in electroanalysis because they improve the properties of the electrode/solution interface. Many surfactants have been studied, with sodium dodecyl sulfate (SDS) being the most extensively researched. It is an anionic surfactant with a one-of-a-kind molecular structure that includes a hydrophobic tail region, and a hydrophilic anionic charged group [18]. Therefore, surfactants may bind on the electrode's surface, increasing analyte adsorption and the rate of electron transfer between the electrode and the solution, thereby improving the performance of the proposed sensors.

Chitosan is a polysaccharide biopolymer produced industrially by hydrolyzing chitin's aminoacetyl groups. Because of its numerous advantages, including non-toxicity, biodegradability, biocompatibility, rich active groups, ability to produce excellent films, high permeability, and low cost [19], has been widely used in agriculture, industry, biomedicine, and chemical sensors. Chitosan is extracted from shrimp shells in this study. Transition metal complexes immobilized on polymeric matrices are promising eco-friendly catalysts due to the advantageous combination of homogeneous and heterogeneous system properties [20]. For the electrooxidation of formaldehyde, a carbon paste electrode modified with chitosan and nickel was effective [21]. Mao and colleagues [22] described a modified electrode for paracetamol detection based on a chitosan-copper complex. Paracetamol was determined using a composite of MWCNTs, chitosan, and cobalt [23]. However, to our knowledge, no studies have been published that use modified NiNPs-SDS/CS screen-printed electrodes as a new electrochemical sensor for the simultaneous detection of paracetamol and 4-aminophenol in PBS solution.

For the first time, this study describes how to transform screen-printed electrodes with NiNPs-SDS/CS complex into a novel and ultrasensitive nano-composite electrochemical sensor using a simple, effective, two-step electrochemical deposition method for the simultaneous detection of 4-AP and PA in PBS solution. Advanced techniques were used to characterize the nano-composites that were created. Cyclic and differential pulse voltammetry measurements were used to assess the electrochemical performance of our modified (NiNPs-SDS)/CS/SPE electrode. In addition, the fabricated sensors were shown to be suitable for the simultaneous detection of 4-AP and PA in paracetamol tablets with improved stability and excellent reproducibility.

Results and discussion

Chitosan characterization

FT-IR spectroscopy was used to confirm the chemical structure of the extracted chitosan (Fig. 1a). The broader absorption bands at 3100–3500 cm^{-1} were attributed to the stretching vibrations peaks of O–H and N–H. The band at 2866 cm^{-1} is referred to the C–H symmetric stretching vibration [24]. The bands at 1652 cm^{-1} and 1589 cm^{-1} are assigned to the stretching vibrations of C=O from –NHCO– and the bending vibrations of N–H from $–NH_2$, respectively. The bands at 1429 cm^{-1}, 1378 cm^{-1}, and 1149 cm^{-1} are ascribed to amide-I, amide-II, and C–O–C stretching vibration of glycoside linkage. The band at around 1025 cm^{-1} corresponds to the stretching band of the C–O group. The band at 882 cm^{-1} corresponds to the monosaccharide aromatic ring's C–H out-of-plane bending vibration [25].

A scanning electron microscope is used to examine the morphology of the chitosan sample. Chitosan has a very homogeneous surface with a lamellar and dense structure, as shown in the scanning electron microscopy (SEM) micrograph (Fig. 1b).

Structure and morphology of the surface-modified SPE

FESEM was used to characterize the surface morphology of bare SPE (a), CS/SPE (b), NiNPs/CS/SPE (c), and NiNPs-SDS/CS/SPE (d) (Fig. 2). The surface of bare SPE (Fig. 2a) was inhomogeneous and uneven. However, after adding CS (Fig. 2b), the SPE surface became more homogeneous and porous than bare SPE, resulting in a high surface area. The NiNPs-SDS/CS/SPE and NiNPs/CS/SPE structures have a loosely stacked porous structure, possibly due to the porous CS structure (Fig. 2c and d). As a result, it was clear how the anionic surfactant SDS contributed to the deposit's surface texture. Furthermore, negative functional groups may be adsorbed in SDS-containing solutions on Cs/SPE, promoting nickel ion reduction and providing a well-dispersed deposit over the surface's biopolymer [18].

Figure 2e shows the X-ray diffraction (XRD) pattern of the modified NiNPs-SDS/CS/SPE electrode. Peaks at angular positions 26.8°, 44.7°, 54.8°, and 76.5° correspond to hexagonal graphite crystalline planes (002), (101), (004), and (110) (JCPDS No. 00-008–0415). The observed peaks at 2 values of 44.7°, 52.1°, and 76.5° correspond to (111), (200), and (220) cubic phase Ni diffractions, respectively (JCPDS No. 00-004–0850). The reported work [10] is in good agreement with the characteristic Ni peaks. The XRD results confirm that NiNPs were successfully grown on the SPE electrode.

Electrochemical characterization of the surface-modified SPE

The electrochemical properties of various modified electrodes were investigated using cyclic voltammetry (CV) and electrochemical impedance spectroscopy (EIS) techniques in 0.1 M KCl solution with 1.0 mM $[Fe(CN)_6]^{3-}$ as a redox probe. Figure 3a presents the CV curves of bare SPE, CS/SPE, NiNPs/CS/SPE, and NiNPs-SDS/CS/SPE, recorded at a potential sweep from − 0.4 to 0.7 V and acquired at a scan rate of 50 mV s^{-1}. The oxidation and

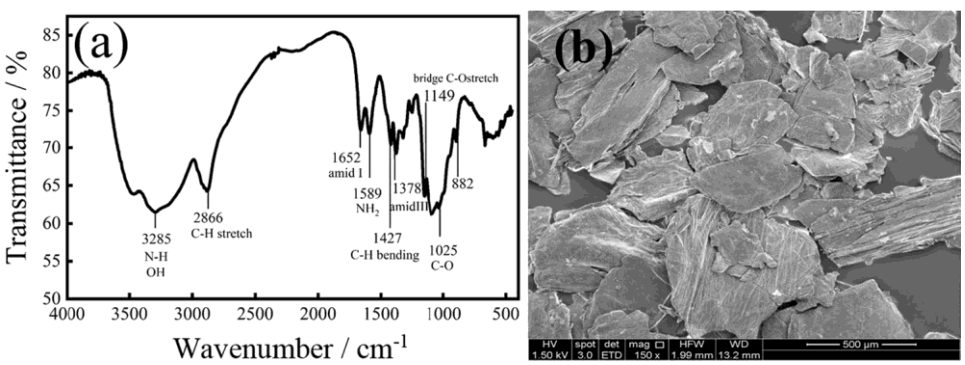

Fig. 1 **a** FT-IR spectrum of prepared chitosan. **b** SEM image of prepared pure chitosan

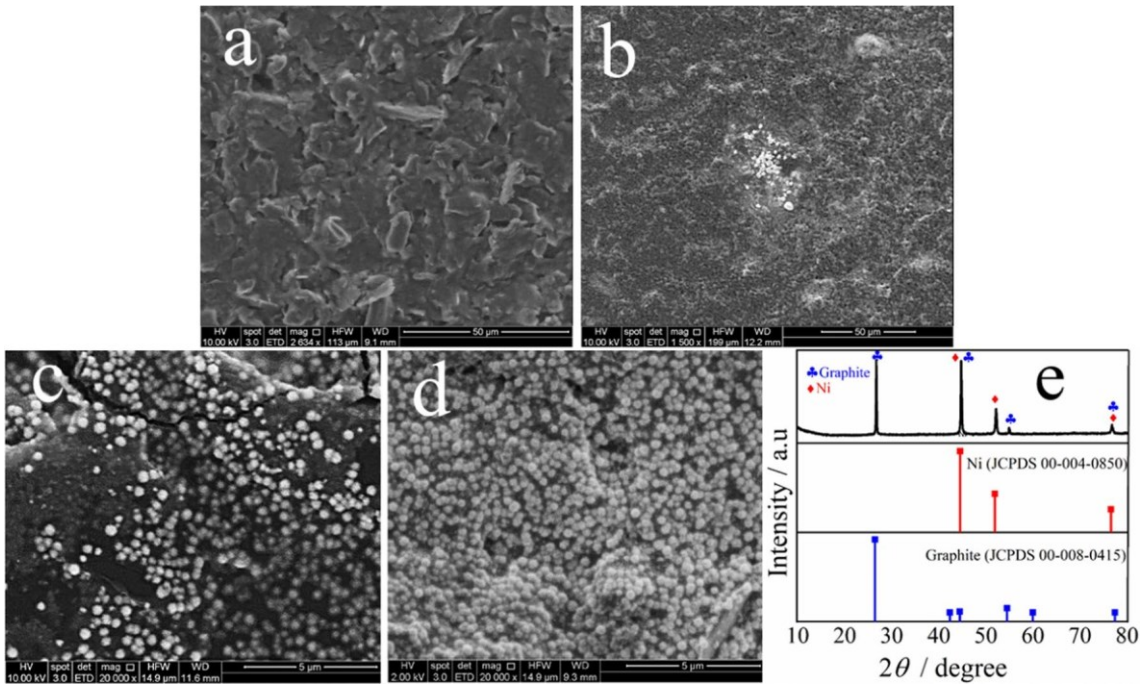

Fig. 2 FE-SEM images of **a** SPE, **b** CS/SPE, **c** NiNPs/CS/SPE, **d** NiNPs-SDS/CS/SPE, **e** XRD pattern of NiNPs-SDS/CS/SPE electrode

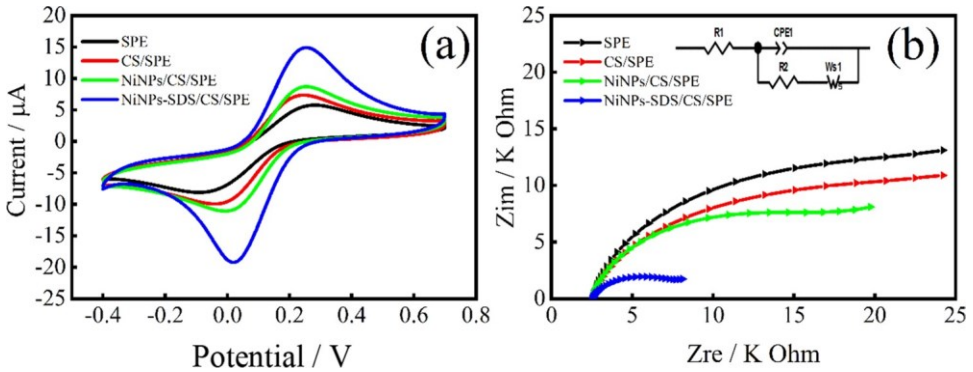

Fig. 3 **a** CV curves and **b** EIS of SPE, CS/SPE, NiNPs/CS/SPE, and NiNPs-SDS/CS/SPE electrodes in 1 mM $[Fe(CN)_6]^{3-}$ solution containing 0.1 M KCl, acquired at a fixed scan rate: 50 mV s^{-1} and frequency range of 100 kHz to 0.1 Hz [Inset: the equivalent circuit]

reduction peak currents of the NiNPs-SDS/CS/SPE are significantly larger than those of the NiNPs/CS/SPE, CS/SPE, and bare SPE (Fig. 3a). These results suggested that the electroactive surface area was increased due to the SPE's modification with CS, NiNPs, and NiNPs-SDS. The peak-to-peak separation between the anodic and cathodic peaks (ΔE_p) for the redox probe at the modified electrodes, and the bare SPE increased in the following trend: 0.235 < 0.255 < 0.286 < 0.304 V respectively for NiNPs-SDS/CS/SPE, NiNPs/CS/SPE, CS/SPE, and bare SPE. Hence, a modified NiNPs-SDS/CS can effectively improve the electrical conductivity and enhance the electron transfer rate.

EIS was also used to compare the performance of unmodified and modified electrodes in the same ferricyanide solution at the frequency range from 100 kHz to 0.1 Hz. The EIS plots of the bare SPE, CS/SPE, NiNPs/CS/SPE, and NiNPs-SDS/CS/SPE in Fig. 3b show a slight semicircle portion in the high-frequency domain demonstrating the electron transfer limited step and the semicircle diameter is equal to the charge transfer resistance (*R*ct), while the linear part with angle 45° assigned to diffusion control of $[Fe(CN)_6]^{3-}$ species at lower frequencies. The impedance data is fitted using the Randles equivalent circuit. In this circuit, R_1, CPE_1, R_2, and WS_1 are referred to as solution resistance, constant phase element, charge transfer resistance, and simulating Warburg element, respectively (see Fig. 3b, inset).

The calculated electron transfer resistance (R_1) values for bare SPE, CS/SPE, NiNPs/CS/SPE, and NiNPs-SDS/CS/SPE were estimated to be 14.88 kΩ (χ^2 = 0.020), 12.42 kΩ (χ^2 = 0.031), 6.29 kΩ (χ^2 = 0.029), and 3.19 kΩ (χ^2 = 0.027), respectively. The results confirm that the modified

NiNPs-SDS/CS/SPE electrode has higher conductivity than other electrodes.

The electroactive surface areas of unmodified SPE and modified SPEs were evaluated from the slopes of the curves $I_p$vs. $v^{1/2}$ (Fig. S1.b, d, f, h), using Randles–Sevcik's equation [26]:

$$I_p = 0.436nFAC\sqrt{\frac{nFDv}{RT}} \quad (1)$$

where n is the number of electrons, I_p is the anodic peak current (A), D is the diffusion coefficient ($cm^2\ s^{-1}$), A is the surface area of the electrode (cm^2), is the scan rate (V s^{-1}), and C is the concentration of $[Fe(CN)_6]^{3-}$ (mol cm^{-3}).

Through the calculation, the effective active surface areas of bare SPE, CS/SPE, NiNPs/CS/SPE, and NiNPs-SDS/CS/SPE were calculated to be 5.2×10^{-2}, 5.6×10^{-2}, 6.2×10^{-2}, and 7.1×10^{-2} cm^2, respectively. This result shows that the NiNPs-SDS/CS complex was successfully grown onto the SPE electrode's surface, increasing the modified electrode's specific surface area and conductivity.

Electrochemical behavior of 4-AP and PA

CV was used to investigate the electrochemical behaviors of 4-AP and PA at various modified electrodes in 0.1 M PBS, individually and simultaneously (pH 7.0). First, the two compounds' individual electrochemical properties were investigated. The cyclic voltammograms of 0.1 mM 4-AP on bare SPE, CS/SPE, NiNPs/CS/SPE, and NiNPs-SDS/CS/SPE are shown in Fig. 4a. It can be seen that the 4-AP redox current peaks are largest at NiNPs-SDS/CS/SPE compared to NiNPs/CS/SPE, CS/SPE, and bare SPE, indicating that the NiNPs-SDS/CS composite has excellent redox performance for 4-AP determination.

The separation of anodic and cathodic peak potentials (ΔE_p) of 4-AP is 61 mV for the NiNPs-SDS/CS, which is lower than those NiNPs/CS/SPE (68 mV), Cs/SPE (71 mV), and bare SPE (76 mV). Similarly, the NiNPs-SDS/CS/SPE displayed a potent ability for PA signal amplification (Fig. 4b). Meanwhile, the peak-to-peak separation (ΔE_p) between the anodic and cathodic peak of PA was decreased to 72 mV compared to 84 mV, 204 mV, and 277 mV for NiNPs/CS/SPE, CS/SPE, and bare SPE, respectively. According to the results mentioned above, the modified electrode improved the reversibility of electrochemical reactions and the electron transfer of 4-AP and PA. The CV responses of a mixture of 4-AP and PA were also examined. The simultaneous study of the mixed solution, like an individual analysis, revealed that the charge transfer during the oxidation of 4-AP and PA was electrochemically quasi-reversible.

The 4-AP and PA response signals on four different modified electrodes increased to varying degrees, with the NiNPs-SDS/CS/SPE electrode exhibiting significantly sharper peaks and higher currents than the other electrodes. Peak potentials must be well separated in simultaneous detection to avoid interference. Anodic peak potential separations of less than 170 mV were discovered in this current study, indicating a significant possibility for simultaneous detection of 4-AP and PA. Based on these findings, the newly NiNPs-SDS/CS-modified screen-printed electrode was selected as the electrocatalytic material for detecting 4-aminophenol and paracetamol individually and simultaneously.

Parameter optimization

pH effect

The effect of electrolyte pH (pH 5–9) on the electrochemical oxidation of 0.1 mM 4-AP and 0.2 mM PA mixture at NiNPs-SDS/CS/SPE was investigated using a CV method. The oxidation peak current of 4-AP and PA increased as the pH value increased to 7 and then decreased when the pH exceeded 7.0 (Fig. 5a and b). As a result, this pH value was used in subsequent experiments. The anodic peak potentials of PA and 4-AP shifted negatively and linearly

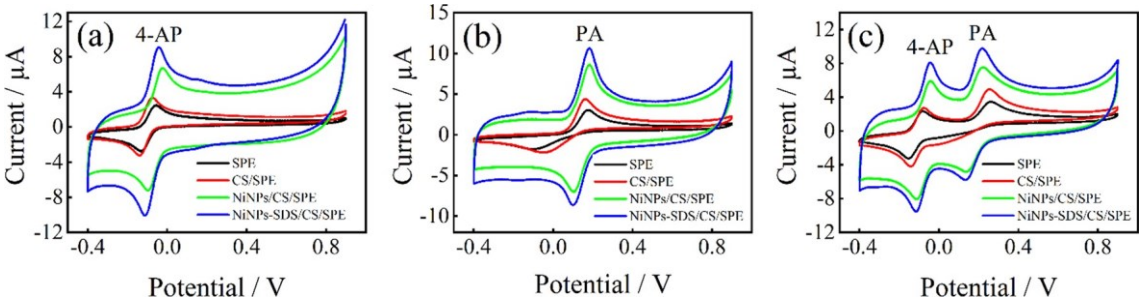

Fig. 4 CV curves of 0.1 mM 4-AP (**a**), 0.1 mM PA (**b**) and the mixture of 0.1 mM 4-AP and 0.1 mM PA (**c**) on bare SPE, CS/SPE, NiNPs/CS/SPE, and NiNPs-SDS/CS/SPE in 0.1 M PBS (pH 7.0) as supporting electrolyte at scan rates of 50 mV s^{-1}

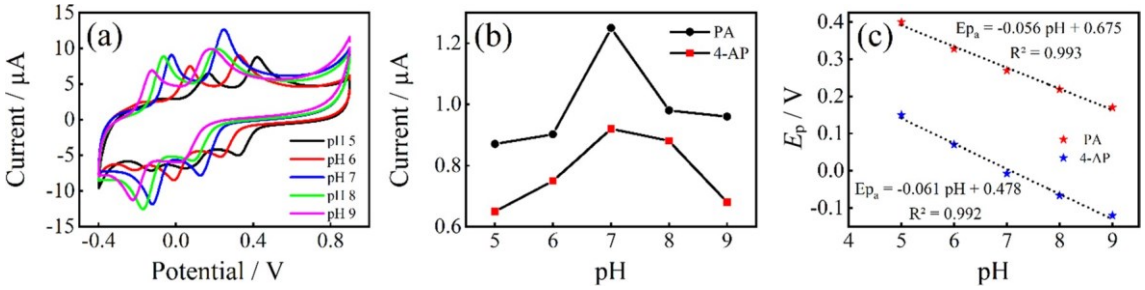

Fig. 5 **a** CVs curves of SPE-modified NiNPs-SDS/CS electrode in 0.1 M PBS containing the mixture of 0.1 mM 4-AP and 0.2 mM PA with different pH values, at scan rate 50 mV s^{-1}. **b** Effect of pH on the oxidation peak current of 4-AP and PA; **c** the dependence of oxidation potential of 4-AP and PA to pH

Scheme 1

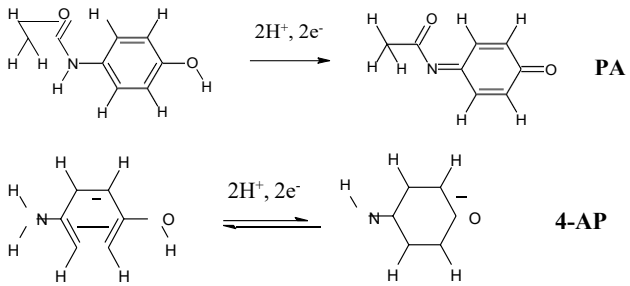

with increasing pH from 5.0 to 9.0, indicating that protons were involved in the electrode reaction (Fig. 5c). The linear regression equations can be displayed as follows: E_{pa} (4-AP) = − 0.061 pH + 0.478 (R^2 = 0.992) for 4-AP and E_{pa} (PA) = − 0.056 pH + 0.675 (R^2= 0.993) for PA. The obtained slopes of 61 mV/pH and 56 mV/pH for 4-AP and PA, respectively, are very close to the Nernstian value of 59 mV/pH, suggesting that the redox process involves two protons and two electrons, which is also supported by the previous studies [27]. The corresponding electrode mechanism is shown in Scheme 1.

Scan rate effect

In order to understand the nature of electrocatalytic process, The effect of scan rates on the redox process of 4-AP and PA on the NiNPs-SDS/CS modified SPE was also investigated by CV at various scan rates ranging from 10 to 300 mVs^{-1}. The redox peak currents of 4-AP and PA increased as the scan rates increased, as shown in (Fig. 6a). Furthermore, the corresponding anodic and cathodic peak potentials shifted slightly to the positive and negative directions, indicating that the modified NiNPs-SDS/CS/SPE in the electrochemical process for 4-AP and PA oxidation has a kinetic limitation.

The anodic and cathodic peak currents of 4-AP and PA were directly proportional to the scan rate's square root (v)

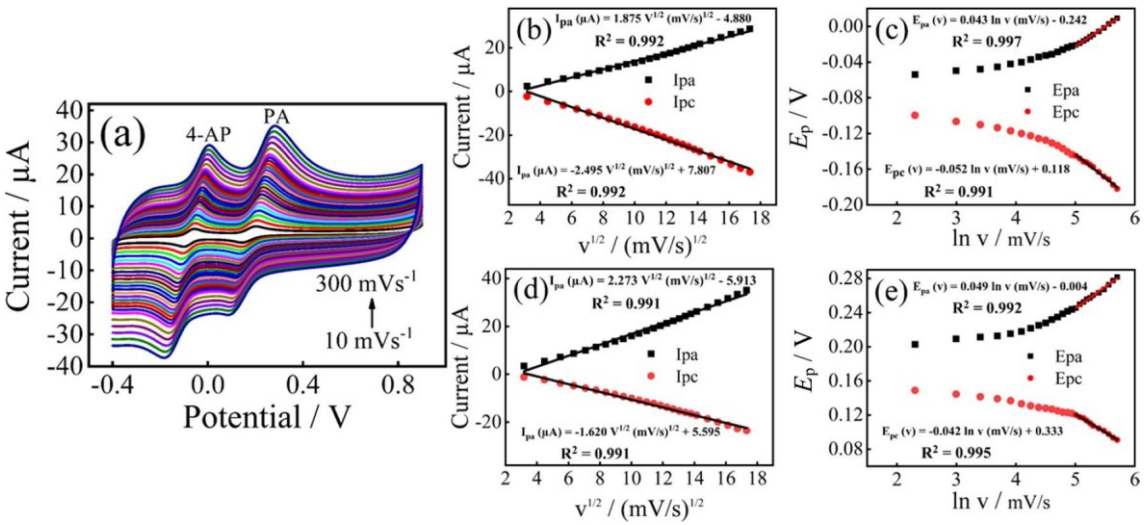

Fig. 6 **a** CVs curves of SPE-modified NiNPs-SDS/CS electrode in the mixture of 0.1 mM 4-AP and 0.1 mM PA at different scan rates (10–300 mVs^{-1}); **b**, **d** Correlation plots of peak currents versus the square root of scan rates; **c**, **e** plots of peaks potential versus ln$v$

ranging from 10 to 300 mV s^{-1} with fitted equations of: I_{pa} (μA) =1.875 $v^{1/2}$ (mV/s)$^{1/2}$ – 4.88 (R^2 = 0.992), I_{pc}(μA) = – 2.495 $v^{1/2}$ (mV/s)$^{1/2}$ + 7.708 (R^2 = 0.992) for 4-AP (Fig. 6b), and I_{pa} (μA) = 2.273 $v^{1/2}$ (mV/s)$^{1/2}$ – 5.913 (R^2 = 0.991), I_{pc} (μA) = – 1.620 $v^{1/2}$ (mV/s)$^{1/2}$ + 5.595 (R^2 = 0.991) for PA (Fig. 6d), respectively. Therefore, it can be noted that the electrode reaction of both 4-AP and PA at modified NiNPs-SDS/CS/SPE is dominated by a diffusion-controlled process.

Figure 6c and e show an excellent linear relationship between anodic and cathodic peak potentials and Napierian logarithm of scan rates (ln$v$) with a high correlation coefficient of 0.99. The equations are expressed as: E_{pa}(V) = 0.043 ln$v$ (mV/s) – 0.242, (R^2 = 0.997) and E_{pc}(V) = – 0.052 ln$v$ (mV/s) + 0.118, (R^2 = 0.991) for 4-AP, and E_{pa}(V) = 0.049 ln$v$ (mV/s) – 0.004, (R^2 = 0.992) and E_{pc}(V) = – 0.042 ln$v$ (mV/s) + 0.333, (R^2 = 0.995) for PA. According to Laviron's theory [28]:

$$E_{pa} = E^0 + A \ln v \quad (2)$$

$$E_{pc} = E^0 + B \ln v \quad (3)$$

$$A = RT/(1-\alpha)nF \text{ and } B = RT/\alpha nF,$$

$$\ln Ks = \alpha\ln(1-\alpha) + (1-\alpha)\ln\alpha - \ln\frac{RT}{nFv} - \frac{\alpha(1-\alpha)nF\Delta E_p}{2.303RT} \quad (4)$$

where E^0 is the formal redox potential, n is the electron transfer number, v is the scan rate, and R, F, and T are constant and retain their standard meanings.

The electrochemical parameters related to the modified electrode, such as electron-transfer coefficient (α) and electron transfer rate constant (Ks), can be calculated from Eqs. (2), (3), and (4). The estimated values of α and Ks of 4-AP and PA were 0.57, 2.79 s^{-1} and 0.44, 3.12 s^{-1}, respectively. The proposed modified electrode revealed higher PA and 4-AP Ks values than those reported by other electrodes in the literature due to the high ability of the Ni nanostructures, which boosted the electron transfer rate between both 4-AP and PA, as well as the modified electrode surface. This finding suggests that the modified electrode facilitates the diffusion-controlled process of both 4-AP and PA.

Individual and simultaneous determination of 4-AP and PA

CV and DPV techniques were used to evaluate the 4-AP and PA sensing applications of developed electrochemical NiNPs-SDS/CS/SPE electrodes. CV was used to test the concentration effect of the 4-AP and PA at the proposed NiNPs-SDS/CS/SPE, as shown in Fig. 7a and b, respectively. Peak currents, in either case, show a steadily increasing analyte concentration. The peak current versus 4-AP concentration plot, as shown in Fig. 7d, demonstrated a good linear relationship for concentrations ranging from 1.0 to 120 μM and from 120 to 500 μM, with the linear equations

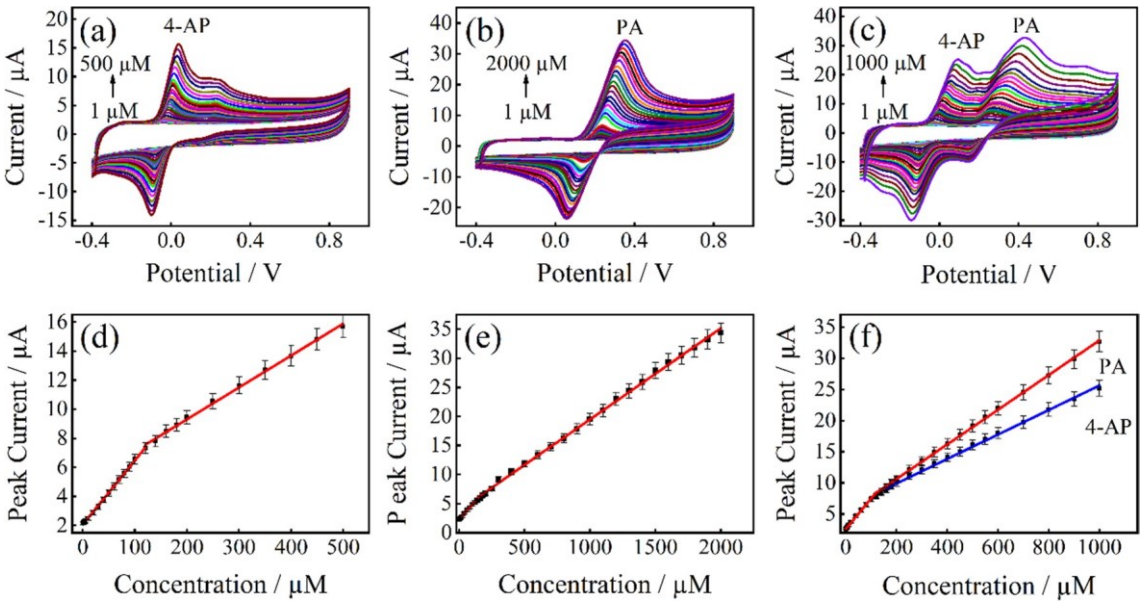

Fig. 7 CVs response for various concentrations of **a** 4-AP, **b** PA, and **c** both 4-AP and PA at modified NiNPs-SDS/CS/SPE sensor in 0.1 M PBS (pH 7.0) solution at 50 mV s^{-1}. **d**, **e** and **f** show the plots of I_{pa}vs. concentration. Error bars come from the average of triplicate replicates (RSD)

for these ranges being: I_{pa} (μA) = 0.044 C (μM) + 2.07 (R^2 = 0.999), and I_{pa} (μA) = 0.022 C (μM) + 4.93 (R^2 = 0.998), respectively.

The new sensor's corresponding detection limit (LOD) (S/N = 3) was calculated to be 1.29 μM. Two linear responses for the PA analyte ranged from 1 to 120 μM and 120 to 2000 μM (Fig. 7e), respectively, as demonstrated by the linear equations: I_{pa} (μA) = 0.025 C (μM) + 2.298 (R^2 = 0.998) and I_{pa} (μA) = 0.016 C (μM) + 3.785 (R^2 = 0.999). The detection limit was found to be 1.42 μM. The sensitivity of the proposed electrode toward the electrooxidation of 4-AP and PA was calculated to be 0.62 ± 0.051 and 0.356 ± 0.048 μA μM^{-1} cm^{-2}, respectively.

In the next step, the analytical performances of the proposed sensor for the simultaneous determination of 4-AP and PA were investigated by CV. The current peak of 4-AP was clearly separated from that of PA (Fig. 7c), and the oxidation peak currents increased accordingly. As a result, the calibration plots for both analytes are linear over two linear responses ranging from 1 to 100 μM and 100 to 1000 μM, respectively (Fig. 7f). The calibration plots and correlation coefficients are written as follows: I_{pa} (μA) = 0.048 C (μM) + 2.696 (1–100 μM, R^2 = 0.998) and I_{pa} (μA) = 0.02 C (μM) + 5.972 (100–1000 μM, R^2= 0.998) for 4-AP, and I_{pa} (μA) = 0.05 C (μM) + 2.626 (1–100 μM, R^2 = 0.997) and I_{pa} (μA) = 0.028 C (μM) + 5.05 (100–1000 μM, R^2 = 0.997) for PA.The detection limits for 4-AP were 1.9 μM and 2.4 μM for PA, respectively. The results of the simultaneous detection of both analytes, 4-AP and PA, were similar to those of the individual analysis, demonstrating that the proposed NiNPs-SDS/CS/SPE sensor could detect these two analytes with high sensitivity either individually or simultaneously.

The DPV technique was also used under optimized conditions to evaluate the electrochemical properties of newly proposed NiNPs-SDS/CS/SPE for the simultaneous detection of both 4-AP and PA analytes by keeping one species constant while varying the other. Figure 8a shows the DPVs of different concentrations of 4-AP (0.5–350 μM) in the presence of 10 μM PA at NiNPs-SDS/CS/SPE in 0.1 M PBS (pH 7). The oxidation peak currents increase as 4-AP is sequentially injected, whereas PA's peak currents and peak potentials do not change significantly. The linear responses for 4-AP are displayed as follows: I_p (μA) = 0.068 C (μM) + 0.834 (0.5–10 μM, R^2 = 0.999) and I_p (μA) = 0.016 C (μM) +1.47 (10–300 μM, R^2 = 0.998) (Fig. 8d).The detection limit of 4-AP was found to be 0.06 μM (S/N = 3). The sensitivity for detecting 4-AP and PA was found to be 0.959 ± 0.058 μA μM^{-1} cm^{-2} and 1.163 ± 0.039 μA μM^{-1} cm^{-2}, respectively.

Analogously, Fig. 8b depicts DPV responses for various PA concentrations in the presence of 20 μM 4-AP. The linear response of PA ranged from 0.05 to 400 μM and was presented by the following linear regression equations: I_p (μA) = 0.083 C (μM) + 0.239 (0.05–10 μM, R^2 = 0.999) and, I_p (μA) = 0.012 C +1.064 (μM) (10–400 μM, R^2 = 0.997) (Fig. 8e). PA detection limit was determined to be 0.04 μM (S/N = 3). The simultaneous detection of 4-AP

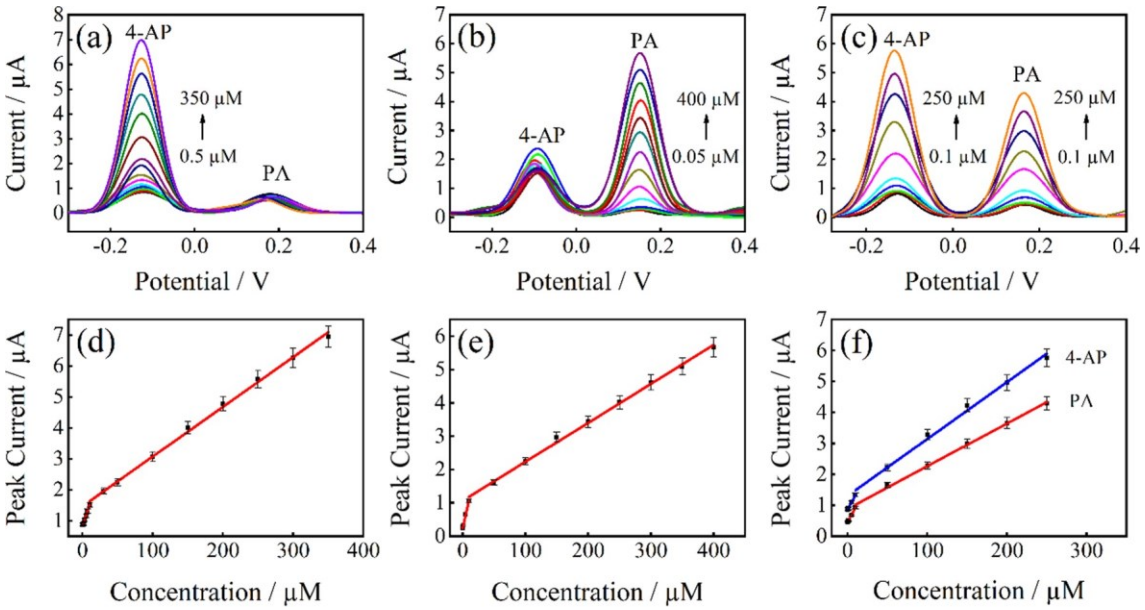

Fig. 8 DPV curves of modified SPE-modified NiNPs-SDS/CS for the mixture of PA and 4-AP in 0.1 M PBS (pH 7.0) solution: **a** 10 μM PA and 0.5–350 μM 4-AP, **b** 20 μM 4-AP and 0.05–400 μM PA, **c** 0.1–250 μM 4-PA and 0.1–250 μM PA. **d**, **e** and **f** show the plots of I_p vs. concentration. Error bars come from the average of triplicate replicates (RSD)

and PA was investigated by varying their concentrations at the same time (Fig. 8c). As can be seen, the peak-to-peak separation (0.428 V) is large enough to determine 4-AP and PA simultaneously. The oxidation peak currents consistently increased, demonstrating a good linear relationship. The linear equations of 4-AP are expressed as follows: I_p (μA) = 0.048 C + 0.856 (0.1–10 μM, R^2 = 0.999), and I_p (μA) = 0.018 C +1.302 (10–250 μM, R^2 = 0.993) (see Fig. 8f). The LOD was found to be 0.087 μM (S/N = 3). The linear equations of PA were displayed by: I_p (μA) = 0.047 C + 0.456 (0.1–10 μM, R^2 = 0.999), and I_p (μA) = 0.014 C + 0.881 (10–250 μM, with R^2 = 0.998) (Fig. 8f). The LOD was calculated to be 0.08 μM (S/N = 3).

Table 1 compares the analytical performances of the proposed NiNPs-SDS/CS/SPE sensor for simultaneously determining both compounds to those of other sensors reported recently in the literature. When compared to other sensors reported in the literature, our constructed sensor has the widest linear range, the lowest limit of detection, and the highest sensitivity for the simultaneous detection of 4-AP and PA, indicating that the newly developed electrode appears to be a promising material for the simultaneous detection of 4-AP and PA.

Reproducibility, repeatability, stability, and interference of the NiNPs-SDS/CS/SPE

The reproducibility, repeatability, stability and interference studies were used to identify the performance of the proposed electrode for sensing application. The reproducibility of NiNPs-SDS/CS/SPE was investigated by analyzing the electrochemical responses of 50 μM 4-AP and 30 μM PA at five NiNPs-SDS/CS modified screen-printed electrodes fabricated using the same process (Fig. S2.a). PA and 4-AP RSD values were found to be 3.2% and 2.8%, indicating that the developed sensor has good reproducibility. The repeatability was investigated by repeating the measurement five times in PBS samples containing the same mixture using the same NiNPs-SDS/CS/SPE sensor (Fig. S2.b). PA and 4-AP RSD values were calculated to be 1.2% and 1.4%, respectively, indicating that the proposed sensor can be used for multiple consecutive measurements.

After 8 weeks of storage at room temperature, the stability of the proposed modified electrode was investigated, and the DPV current response of the proposed NiNPs-SDS/CS/SPE to 40 μM for 4-AP and 100 μM for PA was recorded every week. The oxidation peak current values for PA and 4-AP remained stable (Fig. S2.c) except for a slight current decrease for both molecules. The RSD was found to be

Table 1 Comparison of the proposed NiNPs-SDS/CS sensor's performance with earlier reports for simultaneous 4-AP and PA determination

Electrode	Method	Linear range/μM		Detection limit/μM		Sensitivity/μA μM^{-1}		References
		4-AP	PA	4-AP	PA	4-AP	PA	
AuNPs/CNTs-CONH-TAPP/GCE[a]	DPV	0.08–60	4.5–500	0.44	0.025	0.278	0.0377	[29]
CS/Au/Pd/rGO/GCE[b]	DPV	1.0–300	1.0–250	0.12	0.3	0.0384	0.025	[30]
S-CTFs@$NiCo_2O_4$/GCE[c]	DPV	2–360	2–360	0.35	0.18	0.0654	0.0318	[31]
COF/3D NCNF-T/Au/ GCE[d]	DPV	0.4–340	0.4–320	0.13	0.05	0.0147	0.0097	[32]
PEDOT/GCE[e]	DPV	4–320	1–100	1.2	0.4	0.094	0.284	[33]
AuNPs/SDS-LDH/GCE[f]	DPV	0.5–200	1–400	–	0.13	0.03	0.02	[34]
CdSe/GCE[j]	DPV	1–900	0.5–800	–	0.1	0.0147	0.025	[35]
CS/Ag–Pd@rGO/GCE	DPV	1–300	0.5–300	0.013	0.23	0.024	0.009	[36]
TiO_2 nanoparticle /CPE[h]	CV	–	10–70	–	5.2	–	–	[37]
NiNPs-SDS/CS/SPE	CV	1–120	1–120	1.29	1.42	0.044	0.0157	This work
		120–500	120–2000					
	DPV	0.5–10	0.05–10	0.06	0.04	0.0681	0.0826	
		10–350	10–400					

[a]AuNPs: gold nanoparticles; CNTs-CONH-TAPP: tetraaminophenyl porphyrin functionalized multi-walled carbon nanotubes; GCE: glassy carbon electrodes

[b]CS: Chitosan; Pd: palladium; rGO: reduced graphene oxide

[c]S-CTFs: sulfurbridged covalent triazine frameworks; $NiCo_2O_4$: nickel cobaltite

[d]COF: covalent organic framework; 3D NCNF-T: three-dimensional nitrogen doped carbon nanosheet frameworks

[e]PEDOT: poly(3,4-ethylenedioxythiophene)

[f]SDS-LDH: layered double hydroxide sodium modified with dodecyl sulfate

[j]CdSe: cadmium selenide

[h]CPE: carbon paste electrode

2.9% for 4-AP and 3.1% for PA, indicating that the modified electrode is stable. The DPV technique was also used to test the selectivity of the proposed sensor toward 4-AP and PA in the presence of various interfering species found in paracetamol tablets. The simultaneous detection of 4-AP and PA (peak current change less than 10) was unaffected by the 50-fold concentrations of caffeine (CAF), lactose (LAC), citric acid (CIT), glucose (GLU), and ascorbic acid (AA) (Fig. 9). According to the results, the modified NiNPs-SDS/CS/SPE has excellent selectivity toward 4-AP and PA and no interfering ability.

Real sample analysis

Under optimal conditions, the newly NiNPs-SDS/CS modified screen-printed electrode was used to measure the PA and 4-AP content in two different commercial pharmaceutical samples (500 mg/tablet): PANADOL EXTRA (paracetamol 500 mg + caffeine 25 mg); and DICLOFENAC (paracetamol 500 mg, diclofenac potassium 50 mg) (see sample pretreatment process). The sample was then added to an electrochemical cell containing 0.1 M PBS,

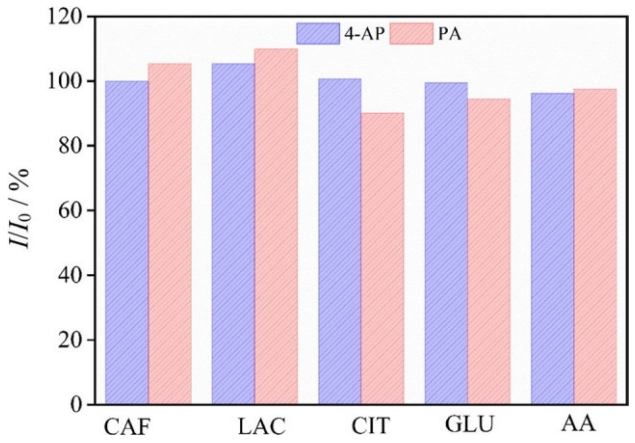

Fig. 9 The effects of some organic molecules on electrochemical determination of 4-AP and PA. *CAF* caffeine, *LAC* lactose, *CIT* citric acid, *GLU* glucose, and *AA* L-ascorbic acid

and the DPV responses of PA and 4-AP oxidation were measured. The relative errors between the results of this work and the nominal value indicated by the pharmaceutical companies are acceptable, as shown in Table 2, and the recovered ranged from 96.8–104.8% for PA to 97–103.5% for 4-AP. On the other hand, caffeine and diclofenac potassium had no effect on the determination of paracetamol in commercial samples using the modified NiNPs-SDS/CS SPE. These findings suggest that the sensor developed in this study has a high potential for detecting paracetamol in pharmaceutical products.

Conclusion

In this work, chitosan-coated nickel nanoparticles were successfully prepared onto a screen-printed electrode by electrodeposition method with the assistance of an anionic surfactant of sodium dodecyl sulfate. The proposed electrode's electrochemical catalytic behavior was investigated using CV and DPV methods. According to the CV results, the novel modified NiNPs-SDS/CS/SPE sensor had the largest linear range, from 1 µM to 2 mM ($R^2 = 0.997$) for PA and 1 to 500 µM for 4-AP ($R^2 = 0.999$), respectively. DPVs response had the highest sensitivity values of 1.163 µA μM^{-1} cm^{-2} for PA and 0.959 µA μM^{-1} cm^{-2} for 4-AP, and the lowest detection limits (LOD) of 0.04 µM and 0.06 µM for PA and 4-AP ($S/N = 3$), respectively.

Kinetic parameters such as the electron transfer coefficient and the heterogeneous rate constant were also determined. The two analytes' distinct and separate peaks at different potentials provide a technique for determining PA in the presence of its toxic degradation product 4-AP and other species. The built electrochemical sensor successfully determined paracetamol in commercial paracetamol tablets without any separation steps, with acceptable recovery and RSD. Therefore, these findings provide a simple and dependable strategy for developing an ultra-sensitive electrochemical sensor for the individual or simultaneous determination of PA and 4-AP in pharmaceutical samples.

Table 2 Determination of 4-aminophenol and paracetamol in pharmaceutical tablets

Samples	PA			4-AP		Recovery/%	
	Reported content/mg per tablet		Determined/mg per tablet	Added/µM	Found/µM	PA	4-AP
PANADOL EXTRA	1	500	498.4	20	18.7	99.7	97
	2	500	492.8	40	39.5	98.6	98.7
	3	500	484.1	60	62.1	96.8	103.5
DICLOFENAC	1	500	511.2	20	19.9	102.2	99.1
	2	500	497.8	40	38.9	99.6	97.2
	3	500	506.8	60	62.9	104.8	98.7

Scheme 2

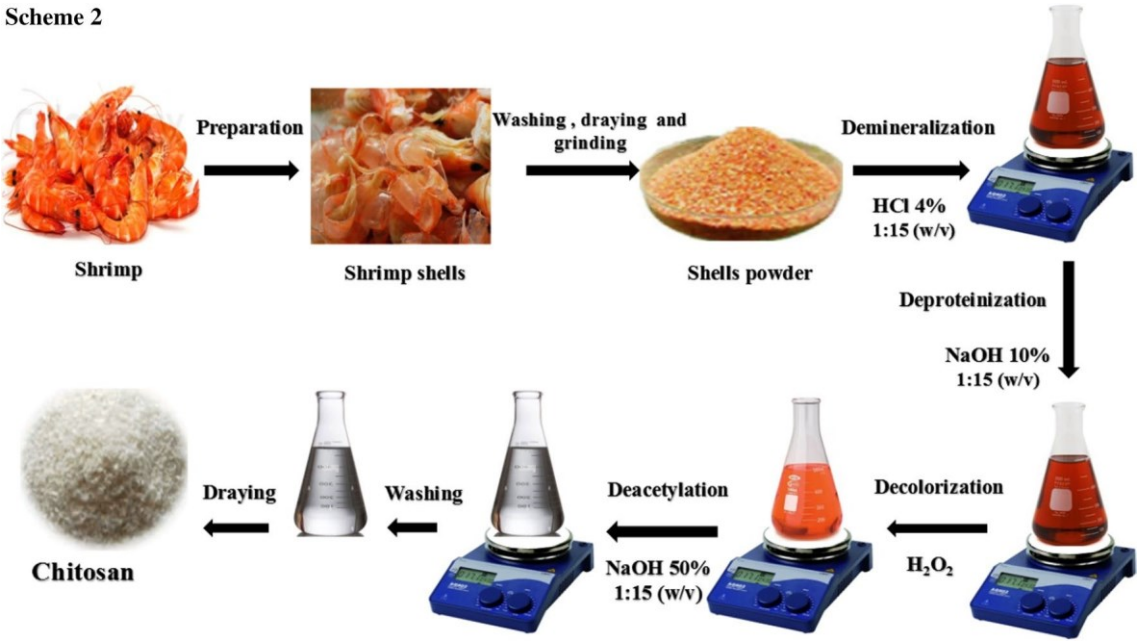

Experimental

Nickel sulfate hexahydrate ($NiSO_4 \cdot 6H_2O$), sodium sulfate (Na_2SO_4), disodium hydrogen phosphate ($Na_2HPO_4 \cdot 2H_2O$), sodium dihydrogen phosphate ($NaH_2PO_4 \cdot 2H_2O$), and sodium dodecyl sulfate (SDS) were obtained from Sigma-Aldrich. Paracetamol (PA), 4-aminophenol (4-AP), L-ascorbic acid (AA), uric acid (UA), caffeine (CAF), lactose (LAC), citric acid (CIT), glucose (GLU), and potassium ferricyanide $K_3Fe(CN)_6$ were purchased from Fluka. All chemicals were analytically pure and purchased without any further purification. Phosphate buffer solutions (PBS, 0.1 M) with pH values ranging from 5 to 9 were prepared. Paracetamol tablets (1000.0 mg per tablet) were purchased from a local pharmacy.

Chitosan polymer (CS) was extracted from shrimp shells using the procedure previously described [25]. In brief, shrimp shells were collected, cleaned, powdered, and then soaked for 24 h in a 4% HCL solution. After that, the powder was treated with a 10% sodium hydroxide (NaOH) solution at 70 °C for 2 h to remove the protein. Decolorization was done with hydrogen peroxide (H_2O_2) and washing with deionized water. The chitin obtained from the above process was deacetylated in 50% NaOH (1:15 w/v) for 3 h at 100 °C and dried to produce chitosan (Scheme 2). Using the Sabnis and Block method based on FT-IR spectroscopy, the degree of deacetylation (DD) was calculated to be 81% [24].

The screen-printed graphite electrodes (SPEs) were manufactured at Manchester Metropolitan University using the required stencil designs and a micro DEK 1760RS screen-printing machine (DEK, Weymouth, UK) [7–9].

Instruments

The structure and morphology of all electrodes were examined using a field emission scanning electron microscope (FE-SEM) with energy dispersive X-ray spectroscopy (EDX) (Quanta FEI-600L). X-ray diffraction (XRD) patterns were obtained by an XRD (Bruker D8 Discover spectrometer, Germany) with Cu-Kα radiation (λ = 1.5418). A Perkin Elmer Spectrum 100 FT-IR spectrometer was used to make FT-IR measurements (KBR pellets). A potentiostat was used in the voltammetric experiments (Princeton Applied Research, AMETEK, USA). SPEs were used for electrochemical measurements, with the fabricated electrodes serving as working electrodes (3 mm diameter), a graphite counter electrode, and an Ag/AgCl pseudo reference electrode. All potentials in this paper are expressed in terms of the SP- Ag/AgCl electrode.

Electrochemical studies

The electrocatalytic performance of modified SPEs towards paracetamol and 4-aminophenol was investigated using CV and DPV measurements. CV measurements were taken at a scan rate of 50 mV s^{-1} in the potential range from − 0.40 to 0.9 V in 0.1 M phosphate buffer solution of pH 7. DPV measurements were performed in the potential range of — 0.40 to 0.5 V with increment potential of 0.005 V, pulse amplitude of 0.05 V, pulse width of 0.2 s, and pulse period of 0.5 s. EIS measurements were carried out in the frequency range of 100 kHz to 0.1 Hz and an amplitude of 10 mV at the formal potential of the $[Fe(CN)_6]^{3-}$ redox couple.

Preparation of the modified electrodes

CS solution (0.5%) was obtained by dissolving 50 mg of chitosan in 10 cm^3 of 1% (v/v) acetic acid solution and sonicating it until complete dissolution. A dilute NaOH solution was used to adjust the pH of the solutions to 4–5. The SPE-modified NiNPs-SDS/CS electrode was elaborated by the following procedure. In the first step, a 5 mm^3 (optimal volume) chitosan solution was manually applied to the SPE surface, dried in the air for 30 min at room temperature, and the electrode was given the designation CS/SPE. The CS/SPE was then immersed in a solution containing 0.1 mol dm^{-3} $NiSO_4$, 0.1 mol dm^{-3} Na_2SO_4, and 0.08 mg cm^{-3} SDS solution in the second step. Five successive voltammetric cycles from − 0.3 to — 1.3 V at a fixed scan rate of 50 mV s^{-1} were used to electrochemically deposit NiNPs-SDS composite on CS/SPE electrode. Finally, to produce constant peak response, the modified NiNPs-SDS/CS/SPE electrode was slightly washed by distilled water and subjected to fifty CV cycles between − 0.4 and 0.9 V in phosphate buffer solution (pH 7). Using the same procedure, the NiNPs-CS/SPE was also developed for comparison.

Real sample

Three tablets of paracetamol (1000 mg/tablet) pharmaceutical formulation were finely ground and precisely weighed in an agate mortar. The sample was then extracted for 30 min with 50 cm^3 ethanol while stirring. After 10 min of centrifugation at 3500 rpm, the filtrate was collected in a calibrated 50 cm^3 flask and diluted with phosphate buffer (0.1 mol dm^{-3}). Then, 50 mm^3 of the above solution was mixed with 4950 mm^3 of PBS for the DPV determination.

Supplementary Information The online version contains supplementary material available at https:// doi. org/ 10. 1007/ s00706-023-03062-7.

Acknowledgements We are very grateful to the financial support within the General Direction of Scientific Research and Technology Development of the Algerian ministry of higher education and scientific research.

Data availability The data that support the findings of this study are available from the corresponding author, upon reasonable request.

References

1. Chetankumar K, Kumara Swamy BE, Sharma SC (2021) Microchem J 160:105729
2. Kenarkob M, Pourghobadi Z (2019) Microchem J 146:1019
3. Nemakal M, Aralekallu S, Mohammed I, Pari M, Venugopala Reddy KR, Sannegowda LK (2019) Electrochim Acta 318:342
4. Sun L, Yang M, Guo H, Zhang T, Wu N, Wang M, Yang F, Zhang J, Yang W (2022) Colloids Surf A Physicochem Eng Asp 647:129092
5. Li M, Wang W, Chen Z, Song Z, Luo X (2018) Sens Actuators B Chem 260:778
6. Khaskheli AR, Fischer J, Barek J, Vyskočil V, Sirajuddin, Bhanger MI (2013) Electrochim Acta 101:238
7. Metters JP, Kadara RO, Banks CE (2011) Analyst 136:1067
8. Khairy M, Mahmoud BG, Banks CE (2018) Sens Actuators B Chem 259:142
9. Khorshed AA, Khairy M, Elsafty SA, Banks CE (2019) Anal Methods 11:282
10. Chelaghmia ML, Fisli H, Nacef M, Brownson DAC, Affoune AM, Satha H, Banks CE (2021) Anal Methods 13:2812
11. Mahmoud BG, Khairy M, Rashwan FA, Banks CE (2017) Anal Chem 89:2170
12. Chelaghmia ML, Nacef M, Affoune AM, Pontié M, Derabla T (2018) Electroanalysis 30:1
13. Chelaghmia ML, Nacef M, Fisli H, Affoune AM, Pontié M, Makhlouf A, Derabla T, Khelifi O, Aissat F (2020) RSC Adv 10:36941
14. Chelaghmia ML, Nacef M, Affoune AM (2012) J Appl Electrochem 42:819
15. Nacef M, Chelaghmia ML, Khelifi O, Pontié M, Djelaibia M, Guerfa R, Bertagna V, Vautrin-Ul C, Fares A, Affoune AM (2021) Int J Hydrogen Energy 46:37670
16. Nacef M, Chelaghmia ML, Affoune AM, Pontié M (2019) Electroanalysis 31:113
17. Kihal R, Fisli H, Chelaghmia ML, Drissi W, Boukharouba C, Abdi S, Nacef M, Affoune AM, Pontié M (2022) J Appl Electrochem 53:315
18. Prinith NS, Manjunatha JG (2019) Mater Sci Energy Technol 2:408
19. Yang Y, Wang Q, Qiu W, Guo H, Gao F (2016) Phys Chem C 120:9794
20. Guibal E (2005) Prog Polym Sci 30:71
21. Hassaninejad-Darzi SK (2014) J Electroceramics 33:252
22. Mao A, Li H, Jin D, Yu L, Hu X (2015) Talanta 144:252
23. Akhter S, Basirun WJ, Alias Y, Johan MR, Bagheri S, Shalauddin M, Ladan M, Anuar NS (2018) Anal Biochem 551:29
24. Sabnis S, Block LH (1997) Polym Bull 39:67
25. Ben Seghir B, Benhamza MH (2017) J Food Meas Charact 11:1137
26. Ferrari AGM, Foster CW, Kelly PJ, Brownson DAC, Banks CE (2018) Biosensors 8:53
27. Han HS, You JM, Seol H, Jeong H, Jeon S (2014) Sens Actuators B Chem 194:460
28. Laviron E (1979) J Electroanal Chem 101:19
29. Shi P, Xue R, Wei Y, Lei X, Ai J, Wang T, Shi Z, Wang X, Wang Q, Mohammed Soliman F, Guo H, Yang W (2020) Arab J Chem 13:1040
30. Wang H, Zhang S, Li S, Qu J (2018) Talanta 178:188
31. Sun L, Guo H, Pan Z, Liu B, Wu N, Liu Y, Lu Z, Wei X, Yang W (2022) Microchem J 182:107879
32. Guan Q, Guo H, Wu N, Cao Y, Wang M, Zhang L, Yang W (2021) Colloids Surf A Physicochem Eng Asp 630:127624
33. Mehretie S, Admassie S, Hunde T, Tessema M, Solomon T (2011) Talanta 85:1376
34. Yin H, Shang K, Meng X, Ai S (2011) Microchim Acta 175:39
35. Yin H, Meng X, Xu Z, Chen L, Ai S (2012) Anal Methods 4:1445
36. Dou N, Zhang S, Qu J (2019) RSC Adv 9:31440

37. Manjunatha KG, Swamy BEK, Madhuchandra HD, Vishnumurthy KA (2021) Chem Data Collect 31:100604

Authors and Affiliations

Sarra Abdi[1] · Mohamed Lyamine Chelaghmia[1] · Rafiaa Kihal[1,2] · Craig E. Banks[3] · Alejandro Garcia-Miranda Ferrari[3] · Hassina Fisli[4] · Mouna Nacef[1] · Abed Mohamed Affoune[1] · Mohamed E. H. Benh amza[1]

[1] Laboratory of Industrial Analysis and Materials Engineering, University May 8, 1945 Guelma, P.O.B. 401, 24000 Guelma, Algeria

[2] Abbes Laghrour University Khenchela, Road of Batna, P.O.B 1252, 40004 Khenchela, Algeria

[3] Faculty of Science and Engineering, Manchester Metropolitan University, Chester Street, Manchester M1 5GD, UK

[4] Laboratory of Applied Chemistry, University May 8, 1945 Guelma, P.O.B. 401, 24000 Guelma, Algeria